

Electrochemical Characteristics of Aluminum Sulfide for Use in Lithium Secondary Batteries

**Hiroshi Senoh^{1,*}, Tomonori Takeuchi¹, Hiroyuki Kageyama¹, Hikari Sakaebe¹, Masaru Yao¹, Koji Nakanishi², Toshiaki Ohta², Tetsuo Sakai¹,
Kazuaki Yasuda¹**

1)Research Institute for Ubiquitous Energy Devices, National Institute of Advanced Industrial Science and Technology (AIST) 1-8-31 Midorigaoka, Ikeda, Osaka 563-8577, Japan

2)Synchrotron Radiation Center (SR Center), Ritsumeikan University, 1-1-1 Noji-Higashi, Kusatsu, Shiga 525-8577, Japan

Abstract

Aiming at a lithium secondary battery with high energy density, aluminum sulfide (Al_2S_3) was studied for use as an active material. The measured initial discharge capacity of Al_2S_3 was ca. 1170 mAh g^{-1} at 100 mA g^{-1} . This corresponds to 62% of the theoretical capacity for the sulfide. Al_2S_3 exhibited poor capacity retention in the potential range between 0.01 and 2.0V, mainly due to the structural irreversibility of the charge process or Li extraction. XRD and Al and S K-XANES analyses indicated that the surface of Al_2S_3 reacts reversibly during charge and discharge processes, while the core of Al_2S_3 showed structural irreversibility because LiAl and Li_2S were formed from Al_2S_3 at the initial discharge and remained as they were afterward.

The paper has been published in J. Power Sources **195** (2010) pp. 8327-8330.

*Corresponding author. Tel.: +81 72 751 9653, fax: +81 72 751 9629

E-mail address: h.senoh@aist.go.jp (H. Senoh)

1. Introduction

Lithium secondary batteries are widely used as electric power sources. To improve battery performance, various active materials have been investigated. Metal sulfides have been proposed as promising active materials because of their high theoretical capacities in comparison to those of currently available systems with oxide-based materials. Recently, a variety of transition metal-containing sulfides MS_2 such as $M = Fe, Co, Ni$ and Cu have been studied [1-4].

With respect to *p*-block elements, some sulfides act as semiconductors. In the field of electrochemistry, lithium-containing sulfide glasses such as $Li_2S-SiS_2-P_2S_5$ and $Li_2S-SiS_2-Al_2S_3$ systems show higher ionic conductivity than the corresponding oxide glasses, which have been studied as candidates for application to solid-state electrolyte materials in lithium secondary batteries [5-9]. By taking advantage of its high ionic conductivity, GeS_2 has been considered as a new anode material for these batteries [10].

In this work, sulfide of lighter element Al was studied. Although the electrochemical behaviors of Al_2S_3 in molten salts have been reported [11,12], to our knowledge, there is no report available on the possible application of Al_2S_3 as an active material for use in lithium secondary batteries. If we assume that Al_2S_3 is completely lithiated ($Al_2S_3 + 10.5Li^+ + 10.5e^- \leftrightarrow 0.5Li_9Al_4 + 3Li_2S$), the theoretical capacity is 1874 mAh g^{-1} or 4123 mAh cm^{-3} . In the present work, we examined the electrochemical properties of Al_2S_3 , particularly focused on the structural change during galvanostatic cycle.

2. Experimental

Commercially available Al_2S_3 powder (purity > 99%, Alfa) was used as-received for electrochemical studies. SEM observation indicated that the Al_2S_3 powder was a lump-like structure with a size of ca. 10 μm . A working electrode was prepared by mixing 3.5 mg Al_2S_3 powder with 1.5 mg teflonized acetylene black (TAB-2, Hohsen), and the resultant electrode was then dried in vacuo for 1 h. A charge-discharge cycle test was performed in a two-electrode system using a sealed cell (HS cell, Hohsen). The counter electrode was Li foil (Honjo), and the potential of the working electrode as a positive electrode is represented against (Li/Li⁺). The separator and electrolyte were a porous polypropylene sheet (Asahi Kasei Chemicals) and 1 mol L^{-1} lithium hexafluorophosphate in a 1:1 mixture of ethylene carbonate and dimethyl carbonate (Kishida), respectively. The cell was constructed in an Ar-filled glove box. The cycle test was conducted at 30°C using a charge/discharge unit (TOSCAT-3100, Toyo System). In the cycle test, the prepared cell was first discharged at a current density of 100 mA g^{-1}

with a cutoff potential of 0.01 V, allowed to rest for 1 h, and then charged at the same current density with a cutoff potential of 2.0 V.

After cycle test, the cells were disassembled inside the Ar glove box and the working electrodes were washed with dimethyl carbonate to remove the electrolyte. Ex situ X-ray diffraction (XRD) of the electrode was performed by covering with a cellulose acetate film to avoid a reaction with moisture/air. The XRD patterns were recorded with an XRD unit (X' Pert PRO MPD, PANalytical) using $\text{CuK}\alpha$ radiation. Valence states of elements (Al and S) were examined by Al K-edge and S K-edge X-ray absorption near edge structure (XANES) analyses. The XANES measurements were performed at BL-10 of the SR center, Ritsumeikan University [13].

3. Results and Discussion

Figure 1 shows discharge and charge curves of Al_2S_3 electrode into which teflonized acetylene black has been incorporated. Before the initial discharge, there is no plateau region in a potential window of 2.0-4.0 V. In Fig. 1, the initial discharge curve shows a short plateau at ca. 0.6 V followed by a long plateau at ca. 0.5 V. The former shoulder is observed only at the initial discharge and is enlarged by incorporating the teflonized acetylene black. For an acetylene black, it is reported the SEI formation occurs at the initial discharge [14].

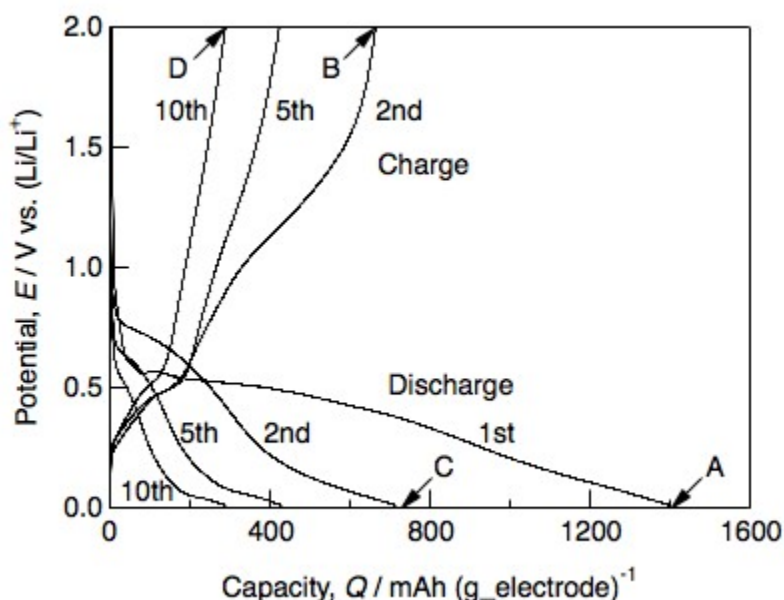


Figure 1 Initial, second, fifth and tenth discharge-charge curves of Al_2S_3 electrode in a potential window of 0.01-2.0 V at 100 mA g^{-1} . Notations A-D correspond to those in Figs. 4, 5 and 6.

The potential decreases smoothly and the initial discharge capacity of the electrode was ca. 1390 mAh g⁻¹. In subsequent charging (second charge), the potential increases gradually. After then, two sloping plateaus are observed at ca. 0.5 V and 1.2 V during charge and two sloping plateaus are also seen at ca. 0.1 V and 0.7 V during discharge. With an increase in the cycle number, all plateau regions, particularly at higher plateaus during both discharge and charge, become narrow.

Capacity retention of Al₂S₃ after subtracting the capacity contribution from teflonized acetylene black is shown in Figure 2. Initial discharge capacity of Al₂S₃ was ca. 1170 mAh g⁻¹. This is about 62% of the theoretical capacities for Al₂S₃. The subsequent charge capacity was ca. 650 mAh g⁻¹, which corresponds to the extraction of 3.6Li. This value is somewhat higher than the capacity of GeS₂ [10]. With an increase in the cycle number, the capacities of Al₂S₃ during both discharge and charge degraded very rapidly to only ca. 240 mAh g⁻¹ after 10 cycles. A notable point is that the discharge capacity remains comparable to the preceding charge; i.e., the coulomb efficiency of discharge against charge is almost 100%. This suggests that the drastic decrease in capacity with cycle is mainly due to the charge process or Li extraction.

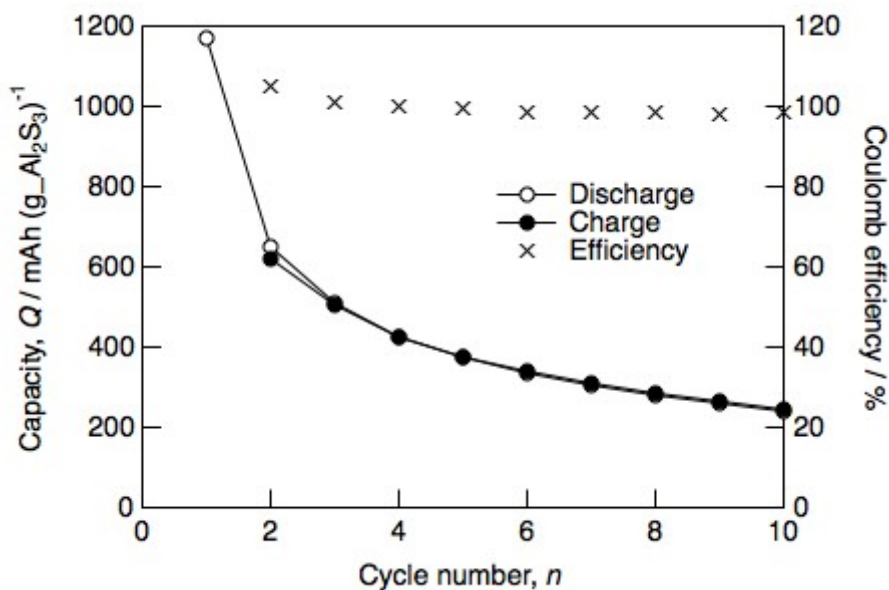


Figure 2 Discharge and charge capacities at 100 mA g⁻¹ corrected for teflonized acetylene black and coulomb efficiency vs. cycle number for Al₂S₃.

Figure 3 shows the rate capability of Al₂S₃. The initial discharge capacity at 1000 mA g⁻¹ is only 33% of that at 100 mA g⁻¹. Below 500 mA g⁻¹, the initial discharge

capacities show an approximately linear dependence with the current density. Discharge capacities that do not include the influence of the overpotential were estimated by extrapolation to 0 mA g^{-1} . The value obtained (1240 mAh g^{-1}) is still far from the theoretical capacity; i.e., Al_2S_3 do not react completely during the initial discharge.

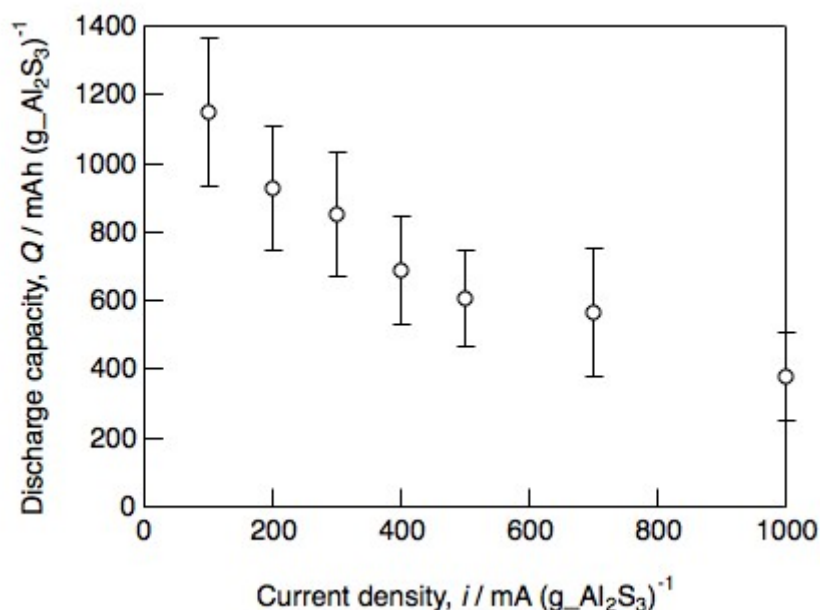


Figure 3 Initial discharge capacity of Al_2S_3 corrected for teflonized acetylene black against current density. Error is twice of the standard deviation of the means values.

To clarify a reaction mechanism and a degradation factor of the electrode, it is important to understand the structural change of Al_2S_3 during discharge and charge. Figure 4 shows ex situ XRD profiles of Al_2S_3 electrode. Before the cycle test (Fig. 3 Before), all diffraction peaks of Al_2S_3 are indexed according to hexagonal structure ($P6_1$) [15]. At the end of initial discharge (A), the diffraction peaks of Al_2S_3 decrease while some broad peaks corresponding to Li_2S appear. In subsequent charge (B), the relative intensities for the diffraction peaks of Al_2S_3 increase again, although those of Li_2S still remain. The diffraction peaks after second discharge (C) are almost identical to those after the initial discharge (A). Li_2S as well as Al_2S_3 remain even in the charged state after 10 cycles (D). Additionally one broad peak (* in Fig. 4 D) was observed at ca. 39° . This may be assigned to Al metal or Li-Al alloy because Al and Li-Al alloy show the strongest peaks around the broad peak (Al(111): 38.6° , LiAl(220): 40.0° , $\text{Li}_9\text{Al}_4(-611)$: 39.1°) [16].

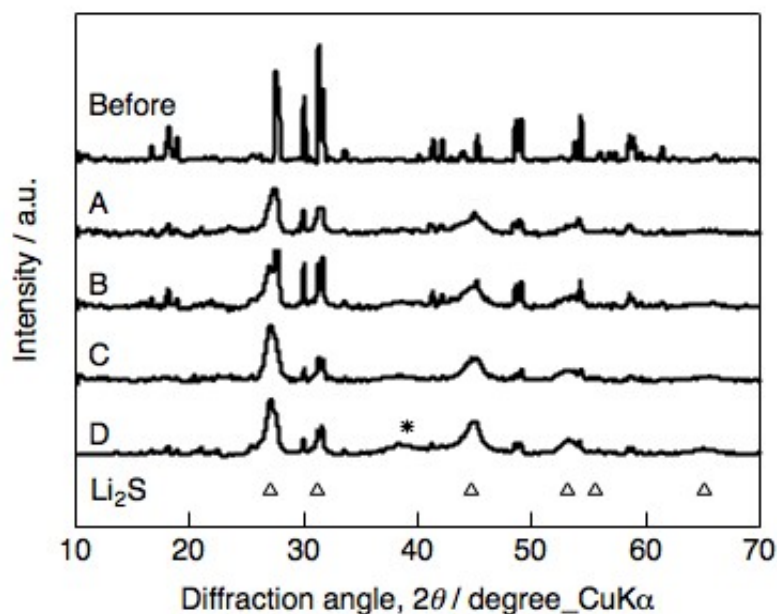


Figure 4 Ex situ XRD profiles of Al_2S_3 electrode before cycle test and after discharge and charge. Notations A-D correspond to those in Fig. 1.

More detailed structural changes were examined by XANES analysis. Figure 5 shows ex situ Al K-edge XANES spectra for the Al_2S_3 electrode obtained with the partial fluorescence yield (PFY) mode before and after the cycle test. In Fig. 5 (a), the edge position shifts to lower energy after the initial discharge (A), and remains at the same energy in the subsequent charge (B). At the second discharge (C), further reduction of the Al_2S_3 electrode occurs. First differential XANES spectra (Fig. 5 (b)) indicate that a peak at around 1562 eV corresponding to Al_2S_3 decreases, while peaks at around 1558 eV and 1559 eV related to Al metal appear after the cycle test. Since the PFY mode is rather bulk sensitive, above results suggest that, in the bulk of Al_2S_3 , the average oxidation state of Al decreases with the first Li insertion probably due to the formation of Li-Al alloy and it remains after the following cycles.

Figure 6 shows ex situ S K-edge XANES spectra for the Al_2S_3 electrode before and after the cycle test. Characteristic absorption peaks at around 2473 eV are originated from S $1s \rightarrow 3p$ electronic transition. The behaviors in the S K-edge XANES spectra measured with the PFY mode (Fig. 6 (a)) are, on the whole, quite similar to those for the Al K-edge XANES spectra. The spectrum after the initial discharge (A) is similar not to that for Al_2S_3 but to that for Li_2S . No significant change of XANES spectra after the second cycle (B and C) suggests that S valence is invariant during the cycle test. In

contrast, the difference in the spectra between discharge and charge is clearly observed with the total electron yield (TEY) mode (Fig. 6 (b)). The peak at around 2473 eV shifts slightly to high energy and its intensity increases after the initial discharge (A).

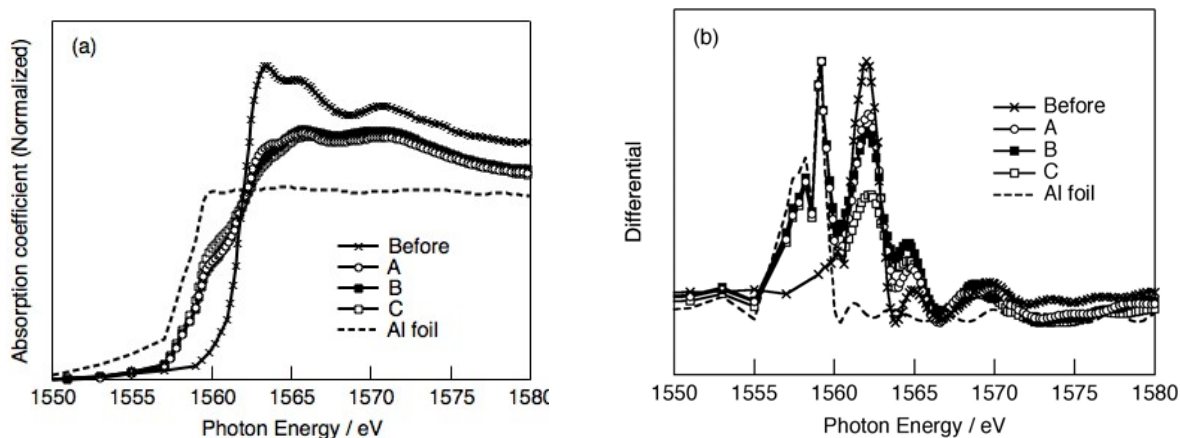


Figure 5 Al K-edge XANES spectra for Al_2S_3 electrode in PFY mode before cycle test and after discharge and charge; normalized (a) and first differential (b). Notations A-C correspond to those in Fig. 1. Al foil was used as a reference.

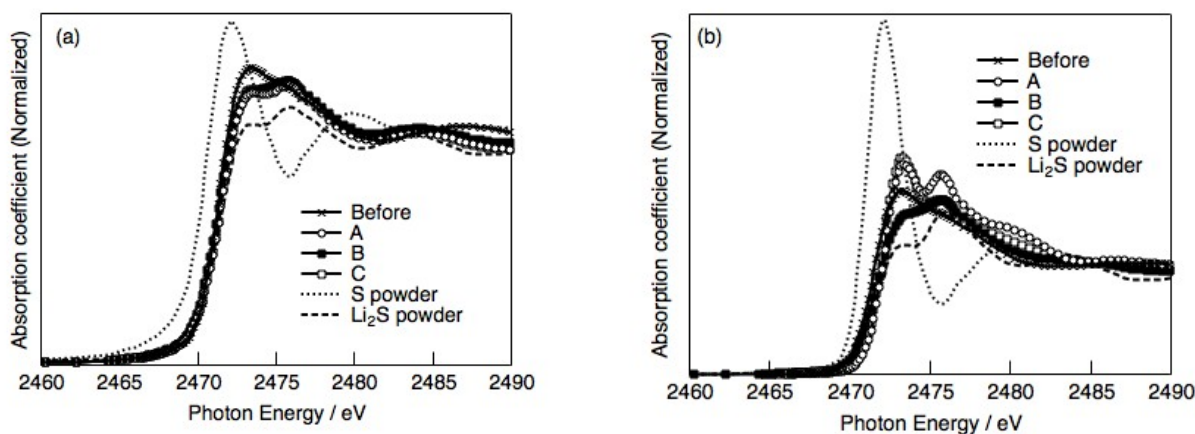


Figure 6 S K-edge XANES spectra for Al_2S_3 electrode in PFY mode (a) and TEY mode (b) before cycle test and after discharge and charge. Notations A-C correspond to those in Fig. 1. Li_2S and S powders were used as references.

Note that the TEY mode is surface sensitive, probing surface atoms in ~ 10 nm. These suggest that, on the surface of Al_2S_3 , the average oxidation state of S increases probably due to the formation of $\text{Li}_2\text{S}-\text{Al}_2\text{S}_3$ alloy such as LiAl_4S_7 and LiAlS_2 . The

change of local structure during the initial discharge may influence the S K-edge XANES spectra. The intensity of the peak around 2476 eV related to Li_2S increases during discharge (A) and decreases again at recharge (B) although the spectrum of the recharged electrode does not completely overlap with that of the original Al_2S_3 electrode. The peak at around 2473 eV after second discharge (C) returns approximately to that after the initial discharge (A). This indicates a reversible reaction on the electrode surface. As shown in Fig. 6, all the spectra have higher edge energy than that for S powder, which indicates the absence of S residue after the cycle test.

Based on the above information, it is reasonable to speculate that the reaction mechanism for Al_2S_3 mainly consists of two steps; $\text{Al}_2\text{S}_3 + 6\text{Li}^+ + 6\text{e}^- \rightarrow 2\text{Al} + 3\text{Li}_2\text{S}$ and $\text{Al} + x\text{Li}^+ + x\text{e}^- \rightarrow \text{Li}_x\text{Al}$. At the initial discharge, Al_2S_3 is converted into Li_2S and Li_xAl (Li-Al alloy). For a Li-Al system, Jow and Laing [17] have reported the effect of composition on the electrode potential of Li-Al alloy. In the present study, the discharge-charge curves with a pair of plateaus below 0.5 V in Fig. 1 approximately agree with the electrode potential reported by them, and an equilibrium potential after the initial discharge (ca. 0.15 V) corresponds to the stability region of the LiAl phase in the Li-Al system. This indicates that the composition of Li-Al alloy is probably not Li_9Al_4 ($x = 2.25$) but LiAl ($x = 1$) and a reaction $\text{Al} + \text{Li}^+ + \text{e}^- \leftrightarrow \text{LiAl}$ occurs at lower potential during charge and discharge. For the higher plateaus during charge and discharge, the midpoint between the potentials (0.7 V and 1.2 V) shown in Fig. 1 is in fair agreement with the equilibrium potential of the reaction $\text{Al}_2\text{S}_3 + 6\text{Li}^+ + 6\text{e}^- \leftrightarrow 2\text{Al} + 3\text{Li}_2\text{S}$ (1.01 V at 25°C), calculated from thermodynamic data [18,19]. In addition, the equilibrium potential of $\text{Li}_2\text{S}/\text{S}$ is 2.25V [20], which is greater than the potential window in the present study. These suggest that the reaction $\text{Al}_2\text{S}_3 + 6\text{Li}^+ + 6\text{e}^- \leftrightarrow 2\text{Al} + 3\text{Li}_2\text{S}$ occurs at higher potential during charge and discharge.

As mentioned above, the drastic decrease in capacity during cycle test is mainly due to Li extraction. From XRD and XANES analysis, it is considered that the surface of Al_2S_3 reacts reversibly during charge and discharge, while the core of Al_2S_3 showed structural irreversibility because LiAl and Li_2S formed from Al_2S_3 at initial discharge remained. The diffusion of Li in LiAl alloy is quite slow [17], which leads to the poor reactivity of Li. Moreover, Li_2S show no significant capacity (electrochemically inactive) due to poor electronic conductivity [21]. The partial solubility of Li_2S into the electrolyte may be another factor in the fading of capacity retention [20]. As shown in Fig. 1, the higher plateaus become particularly narrower during both discharge and charge, which is attributed to the irreversible reaction of Li_2S . These would be responsible for the degradation of the cycle capability in the present Li / Al_2S_3 cells. Therefore, finer Al_2S_3

particles would be anticipated to suppress the formation of LiAl and/or Li₂S and improve the cycle capability, keeping the high initial discharge capacity after subsequent charge and discharge processes. We are currently underway for preparing finer Al₂S₃ particles.

4. Summary

The electrochemical characteristics of Al₂S₃ for use in lithium secondary batteries were investigated using galvanostatic cycle. The prepared electrode showed a high initial capacity although the capacity retention was insufficient. It is reasonable to speculate that the reaction mechanism for Al₂S₃ mainly consists of two steps; Al₂S₃ + 6Li⁺ + 6e⁻ ↔ 2Al + 3Li₂S and Al + Li⁺ + e⁻ ↔ LiAl. The lithiated reaction of Al₂S₃ occurs at low potential, which is a good reason for selecting the sulfide as an anode material.

Acknowledgements

The authors are grateful to their colleagues at the Research Institute for Ubiquitous Energy Devices for their helpful suggestions and stimulating discussions, especially Dr. N. Fujiwara, Dr. T. Ioroi, Dr. Z. Siroma, Dr. S. Yamazaki and Dr. N. Takeichi. We also wish to thank Ms. J. Hirai and Mr. S. Ohta for their helpful assistance. Part of this work was financially supported by the R&D project for Li batteries by NEDO.

References

- [1] R. Fong, J.R. Dahn, C.H.W. Jones, *J. Electrochem. Soc.* **136** (1989) 3206-3210.
- [2] A. Débart, L. Dupont, R. Patrice, J.M. Tarascon, *Solid State Sci.* **8** (2006) 640-651.
- [3] J.M. Yan, H.Z. Huang, J. Zhang, Z.J. Liu, Y. Yang, *J. Power Sources* **146** (2005) 264-269.
- [4] T. Takeuchi, H. Sakaebe, H. Kageyama, T. Sakai, K. Tatsumi, *J. Electrochem. Soc.* **155** (2008) A679-A684.
- [5] E.E. Hellstrom, R.A. Huggins, *Mat. Res. Bull.* **14** (1979) 881-889.
- [6] K. Takada, N. Aotani, S. Kondo, *J. Power Sources* **43-44** (1993) 135-141.
- [7] S.M. Martin, J.A. Sills, *J. Non-Cryst. Solids* **135** (1991) 171-181.
- [8] M. Maruyama, R. Kanno, M. Irie, S. Ito, T. Hata, N. Sonoyama, Y. Kawamoto, *Solid State Ionics* **168** (2002) 140-148.
- [9] A. Hayashi, T. Fukuda, H. Morimoto, T. Minami, M. Tatsumisago, *J. Mater. Sci.* **39** (2004) 5215-5127.
- [10] Y. Kim, H. Hwang, K. Lawler, S.W. Martin, J. Cho, *Electrochim. Acta* **53** (2008) 5058-5064.
- [11] N.Q. Minh, R.O. Loutfy, N.P. Yao, *J. Electroanal. Chem.*, **131** (1982) 229-242.

- [12] V.A. Dusheiko, *J. Power Sources*, **97-98** (2001) 555-556.
- [13] K. Nakanishi, T. Ohta, *J. Phy.: Condens. Matter* **21** (2009) 104214.
- [14] M.V.V.M. Satya Kishore, U.V. Varadaraju, *J. Power Sources* **156** (2006) 594-597.
- [15] B. Krebs, A. Schiemann, M. Laege, *Z. Anorg. Allg. Chem.* **619** (1993) 983-988.
- [16] A.V. Trifonova, A.A. Momchilov, B.L. Puresheva, I. Abrahams, *Solid State Ionics* **143** (2001) 319-328.
- [17] T.R. Jow, C.C. Liang, *J. Electrochem. Soc.* **129** (1982) 1429-1434.
- [18] J.G. Speight Ed., *Lange's Handbook of Chemistry, 16th ed.*, McGraw-Hill, New York, 2005.
- [19] The Electrochemical Society of Japan Ed., *Kagaku-Binran, 5th ed.*, Maruzen, Tokyo, 2000.
- [20] T. Takeuchi, H. Sakaebe, H. Kageyama, H. Senoh, T. Sakai, K. Tatsumi, *J. Power Sources* **195** (2010) 2928-2934.
- [21] M. N. Obrovac, J. R. Dahn, *Electrochem. Solid State Lett.* **5** (2002) A70-A73.